

Table des matières

1	Evaluating and improving cold pools parameterization	1
1.1	Introduction	2
1.2	Tools and methods	4
1.2.1	The LMDZ climate model and its single-column version	4
1.2.2	The cold pools model	5
1.2.3	Large Eddy Simulations : LES	10
1.2.4	High-Tune Explorer (HTEexplo) tool	11
1.3	Analysis of cold pools in the LES	12
1.3.1	Sampling	12
1.3.2	Validation of Phenomenological Laws	22
1.4	Comparison between LES and standard LMDZ	24
1.4.1	The profiles of δT , δq and δw	24
1.4.2	The variables $W A P E$, $A L E_{w k}$, C_* et $A L P_{w k}$	27
1.5	Improvements of cold pools model	27
1.5.1	Coefficient k	28
1.5.2	Altitude h_m	28
1.5.3	The tuning	29
1.5.4	Activation of thermals throughout the domain	32
1.5.5	Effect of changes on $W A P E$, $A L E_{w k}$, C_* and $A L P_{w k}$	33
1.6	Effect of changes on large-scale variables	34
1.7	Conclusions	35

Liste des tableaux

1.1	Comparison of the variables of $WAPE$, ALE_{wk} , C_* and ALP_{wk} calculated in the samplings (E) and those calculated with the formulas of the parameterization (FP) for the coefficient $k = 0.33$ and $k = 0.66$ in the oceanic LES in RCE carried out with SAM and MESONH and in the continental LES of the AMMA case carried out with MESONH	23
1.2	Comparison of the variables $WAPE$, ALE_{wk} , C_* and ALP_{wk} calculated in the LES from the samples and simulated by LMDZ control (LMDZ CTRL) on the oceanic case in RCE and the continental case (AMMA)	28
1.3	List of parameters used for tuning the δT profile	31
1.4	Description of simulations performed with LMDZ in the standard configuration and with various modifications	33
1.5	Comparison of the variables $WAPE$, ALE_{wk} , C_* and ALP_{wk} calculated from the samplings in the LES, with those simulated in LMDZ control (LMDZ CTRL) and with modifications (LMDZ V4)	34

Table des figures

1.1	Conceptual diagram of a density current (Grandpeix and Lafore, 2010).	6
1.2	Map of divergence of wind at 10 m (in s^{-1}) multiplied by 1000 and smoothed horizontally over $3.25 \text{ km} \times 3.25 \text{ km}$ represented on two instants (a and b) of the LES SAM carried out on the oceanic RCE case and superimposed with the contours of temperature anomalies at 10 m at -0.4 K (green), -0.2 K (red) and 0 K (black).	14
1.3	Map of divergence of wind at 10 m (in s^{-1}) multiplied by 1000 and smoothed horizontally over $3.25 \text{ km} \times 3.25 \text{ km}$ represented on the 17 :10 (a) and 18 :00 (b) instants of the LES MESONH carried out on the AMMA case and superimposed with the contours of anomalies of temperature at 10 m at -1 K (green), -0.5 K (red) and 0 K (black).	15
1.4	Vertical profile of condensed water averaged horizontally on the LES in oceanic RCE carried out with the SAM and MésoNH models and the continental LES of the AMMA case carried out with MésoNH.	18
1.5	Maps of anomaly of temperature at 10 m, smoothed horizontally over $2.5 \text{ km} \times 2.5 \text{ km}$, represented on an instant of the LES SAM of the RCE case (a) and on the instant 6 :00 PM of the LES of the AMMA case with black contours indicating thresholds of temperature at 10 m anomaly of -0.2 K (RCE) and -1 K (AMMA). The red color indicates the updrafts on the gust fronts given by the vertical velocities at cloud base (w_b) in the gust fronts mask, which is determined by the w_b smoothed horizontally over $1.25 \text{ km} \times 1.25 \text{ km}$ and exceeding 0.6 m/s (RCE) and over $2 \text{ km} \times 2 \text{ km}$ with a value greater than 2 m/s (AMMA). The green dots represent thermals, defined by w_b outside the gust front mask.	19
1.6	Vertical profiles of the temperature difference between the inside and the outside of cold pools calculated at an instant of the LES (SAM and MESONH) of the RCE case and an instant of the LES MESONH of the AMMA case.	21
1.7	Vertical profiles of δT , δq and δw calculated in the LES and simulated by LMDZ control (LMDZ CTRL) on the RCE case (a, b, c) and on the AMMA case (d, e, f).	26

1.8	Vertical profiles of δT , δq and δw calculated in the LES and simulated in the control LMDZ (LMDZ CTRL), LMDZ with the adjustment of the coefficient k to 0.66 (LMDZ V1), LMDZ with the drop in altitude (h_m) at which the subsidence of the air masses in cold pools is zero (LMDZ V2), LMDZ with the adjustment of the surface fraction of the precipitating descents, σ_{dz} , to 0.02 (LMDZ V3) and LMDZ with the activation of thermals in the entire domain (LMDZ V4) on the RCE case (a, b, c) and on the AMMA case (d, e, f).	30
1.9	Vertical profiles of potential temperature (θ), specific humidity (qv) and cloud fraction (r_{neb}) calculated in the LES and simulated in control LMDZ (LMDZ CTRL), LMDZ with the adjustment of the coefficient k to 0.66 (LMDZ V1), LMDZ with the decrease in altitude (h_m) at which the subsidence of the air masses in cold pools is zero (LMDZ V2), LMDZ with the adjustment of the surface fraction of the precipitating descents, σ_{dz} , to 0.02 (LMDZ V3) and LMDZ with the activation of thermals in all the domain (LMDZ V4) on the RCE case (a, b, c) and on the AMMA case (d, e, f).	36

Chapitre 1

Evaluating and improving cold pools parameterization

1.1 Introduction

During thunderstorms, ~~some of the precipitation may evaporate~~ ^{generally} before reaching the ground, generating cold air masses in the layers below the clouds : the so-called cold pools or wakes. These air masses, denser than their environment, collapse and spread out horizontally. The passage of a cold pool results in a sudden drop in temperature, an acceleration of the wind, a rise in pressure and a change in wind direction (Miller et al., 2008; Allen et al., 2015; Provod et al., 2016; Senghor et al., 2021; McDonald and Weiss, 2021). These cold pool play a key role in maintaining convection, by lifting the surrounding warm air at their gust front initiating new convective cells (Craig and Goff, 1976; Warner et al., 1980; Lima and Wilson, 2008). In organized propagative systems such as squall lines, convective columns are permanently generated by cold pool fronts at the front of the system (Rotunno et al., 1988; Weisman and Rotunno, 2004). Cold pools also play a key role in the self-aggregation of tropical convection (Jeevanjee and Romps, 2013) and in the transition from shallow to deep convection (Khairoutdinov and Randall, 2006; Böing et al., 2012).

^{generating rainfall correctly with parametrized convection is challenging - GCMs are known to often}
In Global Climate Models (GCM), used for climate change studies, convection is parameterized due to the coarse horizontal resolution of these models (30 to 300 km), which does not allow convective and cloudy processes to be explicitly resolved. ~~However, GCMs with parameterized convection underestimate rainfall rates~~ (Pantillon et al., 2015) and produce peak precipitation too early (Randall et al., 2003; Guichard et al., 2004; Yang and Slingo, 2005; Stephens et al., 2010; Dirmeyer et al., 2012). For example, Pantillon et al. (2015), using the Met Office model, showed that peak precipitation occurs at 12 :00 PM with parameterized convection, compared with 05 :00 PM when it is explicitly resolved. They attribute the extension of precipitation into the afternoon, observed in simulations with resolved convection, to the appearance of cold pools. To solve this problem in GCMs, attempts have been made to parameterize cold pools. One of the first attempts to parameterize density currents was proposed by Qian et al. (1998). Later, Grandpeix and Lafore (2010) proposed a parametrization based on a population of identical circular cold pools that are cooled by convective precipitation. The coupling of this parametrization with the deep convection scheme in the LMDZ climate model has significantly improved the representation of convection, particularly the diurnal cycle of precipitation in the tropics (Rio et al., 2009). Although this parametrization of cold pools has led to advances, its internal variables and those used for its coupling with deep convection in LMDZ have not been finely evaluated so far. This is explained not

^{in the day in}
^{at noon in phase with}
maximum insolation, while the maximum peaks ^{generally} in late afternoon or night

④ and depends on the values of a number of free parameters. To explore the sensitivity of those free parameters and refine the model after improvement of its physical content, we use only by a lack of observational data but also by the fact that the internal variables of parameterizations are not directly accessible from observations.

Large Eddy Simulations (LES) are a useful complement to observations, as their very fine horizontal resolution enables them to represent turbulent and convective motions in the boundary layer and associated clouds in explicit detail (Brown et al. 2002; Siebesma et al. 2003). One of the advantages of LES is that they provide three-dimensional information that is not directly available from observations. In addition, they allow the validation of variables internal to the parameterizations, enabling their physical realism to be assessed. They have been used extensively to develop and evaluate boundary layer and convection parameterizations (Rio et al., 2010; Couvreux et al., 2010). In the context of developing cold pool parameterizations, LES are now one of the most commonly used tools (Tompkins, 2001; Khairoutdinov and Randall, 2006; Couvreux et al., 2012; Feng et al., 2015). However, their use for a cold pool assessment remains unexplored. This is due both to the complexity of identifying cold pools in the LES and to the question of which method to use to calculate the internal variables of the cold pools model from the LES. This study aims to evaluate and improve the parameterization of cold pools in LMDZ based on LES.

In the context of improving the physical parameterizations of climate models, a tool for automatic calibration of free model parameters, High-Tune-Explorer, has been developed in recent years (Hourdin et al., 2017). This tool can be used to characterize the subset of parameter values for which the model is in agreement with LES (Couvreur et al. 2020). It will also be used in this study to adjust cold pool model parameters based on LES results.

The paper starts by a presentation of ~~the~~ tools used, including the LMDZ model, cold pools parameterization (Grandpeix and Lafore, 2010), LES, and the tuning tool. In section 2, we detail the sampling carried out to calculate all the cold pools model variables (both internal and those used for coupling with deep convection) in the LES. We also validate the physical laws used to calculate internal variables of cold pools model, based on LES results. Section 3 is devoted to a comparison of cold pools model variables simulated by LMDZ and those calculated in LES, in order to identify the model's limitations. These results will then be discussed, and proposed improvements will be detailed in section 4. Finally, we conclude with a synthesis and discussion of prospects in section 5.

Here we use ~~LES~~ LES to evaluate in detail the parameterization of cold pools in LMDZ. We ~~also~~ first evaluate directly in the LES relationship between ~~some~~ some

We then propose a simulation with LMDZ in SCV parameterization with all the other parameterizations interact with all the other parameterizations. In this case, the parameterization interact with all the other parameterizations.

1.2 Tools and methods

1.2.1 ~~The LMDZ climate model~~ and its single-column version

LMDZ is the Global Climate Model (GCM) used in this work. Developed in the 1970s at the Laboratoire de Météorologie Dynamique (Sadourny and Laval, 1984; Hourdin et al., 2006), the “Z” in LMDZ refers to the model’s ability to refine its horizontal grid over a specific region. This climate model is based on simplified Navier-Stokes equations for fluid mechanics, as well as transport equations. It represents the second generation (Hourdin et al., 2013) of a climate model initially described by Sadourny and Laval (1984). LMDZ is the atmospheric component of the IPSL (Institut Pierre Siméon Laplace) coupled model. The latter is one of around twenty coupled models taking part in major international model intercomparison exercises, such as those of the CMIP (Coupled Model Intercomparison Project), the results of which are used in IPCC (Intergovernmental Panel on Climate Change) reports.

The LMDZ model consists of two main parts, from a physical, mathematical and computational point of view. The first, called “dynamics”, concerns the numerical resolution of the atmospheric general circulation equations. This component manages horizontal exchanges between the model’s grid cells. The second part, called “physics”, calculates the impact of radiation, small-scale processes (subgrid) and phase changes of water on dynamic variables via “physical parameterizations”. This “physical” part is made up of juxtaposed atmospheric columns, which do not interact with each other. Within each column, the variables are assumed to be statistically homogeneous in the horizontal plane.

LMDZ has a single-column version (SCM, Single Column Model). The SCM is built by extracting an atmospheric column from the GCM, incorporating all subgrid-scale parameterizations, and running it in a large-scale constrained environment. This tool is essential for the development and tuning of physical parameterizations in climate models. Parameterizations are developed and evaluated within this single-column framework by comparing them with explicit three-dimensional simulations of the same atmospheric column, where the targeted processes are explicitly resolved. Its low computational cost also allows for a large number of simulations, even on a laptop, making it particularly useful during the development phase, where numerous tests are required.

1.2.2 The cold pools model

The cold pools model represents a population of identical circular cold pools, with the same height, radius, and vertical profiles of thermodynamic variables. Each grid cell in the model is divided into two parts : the first contains cold pools (wake) and the downdrafts, known as precipitating downdrafts. In these downdrafts, the re-evaporation of precipitation generates intense cooling and strong negative buoyancy. A second region, the environment or the exterior of cold pools, contains the warm air that fuels the saturated convective currents (Fig. 1.1). The top of the cold pool (h_{wk}) is defined as the altitude where the temperature inside the cold pool becomes equal to that of the environment. The temperature difference between the cold pool and its environment decreases with altitude ~~due to mass adjustment by gravity waves.~~ Below this level, cold pools collapse and spread out as they are denser than their surroundings. The boundary between the cold pool and the environment is considered to be infinitely thin, and at each point on this boundary, the cold pool spreads at a rate C . C is considered to be a random variable whose mean C_* will give the rate at which the cold pool spreads. In the model, C_* ~~is proportional to~~ ^{scales with} the square root of the potential energy available in the cold pools, or the cold pool's collapse energy, $W A P E$ (Wake Available Potential Energy), since it is assumed that the cold pool's kinetic energy comes from converting this $W A P E$ into kinetic energy.

$$C_* = k\sqrt{2W A P E} \quad (1.2.1)$$

The $W A P E$ is defined as the energy that allows the cold pool to collapse when it becomes denser than its surroundings. It therefore depends ~~very~~ directly on the temperature contrast between the inside and outside of the cold pool. Its expression below is based on Archimedes' principle.

$$W A P E = g \int \frac{\delta \rho}{\bar{\rho}} = -g \int_0^{h_{wk}} \frac{\delta \theta_v}{\theta_v} dz \quad (1.2.2)$$

$$\theta_v = \theta(1 + 0.61q) \quad (1.2.3)$$

where ρ is the air density ; θ_v is the virtual potential temperature ; θ is the potential temperature ; q is the specific humidity.

δX is the difference in the variable X between the inside and outside of cold pools

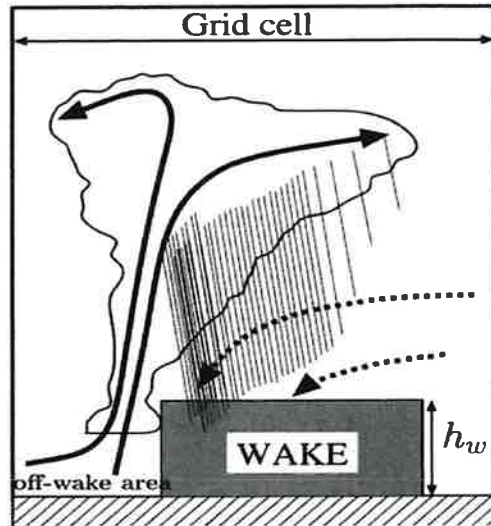


FIGURE 1.1 – Conceptual diagram of a density current (Grandpeix and Lafore, 2010).

and \bar{X} is the mean of the variable X in the domain.

The coefficient k in equation (1.2.1), generally between 0 and 1, depends on the structure of cold pools. Based on 3D CRM (Cloud Resolving Models) simulations, Lafore (2000) (oral communication) estimated this coefficient at 0.33 in the case of a linear structure such as grain lines. This is the value used in the original version of cold pools model.

The spread rate of cold pools is given by C_* from the following relationship :

$$\partial_t \sigma_{wk} = 2\pi r C_* D_{wk} \quad (1.2.4)$$

D_{wk} represents the density of cold pools (number of cold pools per unit area), knowing that the centers are uniformly distributed across the domain.

By introducing the surface fraction $\sigma_{wk} = D_{wk} \pi r^2$ covered by cold pools, the equation 1.2.4 can be reformulated as follows :

$$\partial_t \sigma_{wk} = 2C_* \sqrt{\pi D_{wk} \sigma_{wk}} \quad (1.2.5)$$

Due to the complex life cycle of cold pools (including birth, death, collisions and mer-

gers), calculating their evolution requires an other parameterization. In this study, their density is imposed. In the 6A configuration of LMDZ, this density is imposed at $10 \cdot 10^{-10}$, i.e. 10 cold pools over $100 \text{ km} \times 100 \text{ km}$ over the ocean, while over the continent it is imposed at $8 \cdot 10^{-12}$, i.e. around 8 cold pools over $1000 \text{ km} \times 1000 \text{ km}$. In the model, cold pools initially appear with a surface fraction of 2% and evolve over time according to ~~the~~ equation 1.2.4. ~~However,~~ the evolution of σ_{wk} is arbitrarily limited to a maximum of 40% of the mesh size ($\sigma_{wk} \leq 0.4$).

It is assumed that below the top of cold pool (h_{wk}), the vertical velocity profile associated with the subsidence of the cold pool results solely from the spreading of cold pool at the surface, without lateral entrainment (e_w) or detrainment (d_w) between the cold pool and its environment. Above this top, however, it is assumed that there is lateral entrainment of air into the cold pool, inducing subsidence that gradually ~~decreases~~ ⁱⁿ with altitude up to a height h_m . h_m is considered the altitude above which the thermodynamic differences between the cold pool and the environment become negligible, except within convective currents (saturated currents in the cold pool region, unsaturated descending currents in the environment). In the model, the shape of the vertical velocity difference profile ($\delta\omega$) between the inside and outside of cold pool is imposed as piecewise linear. $\delta\omega$ increases linearly from zero at the surface up to h_{wk} . Between h_{wk} and h_m , $\delta\omega$ decreases linearly. In the version of the model available at the beginning of this study, h_m was set to 600 hPa. In this original version, there was also a nonzero velocity difference ($\delta\omega$) above h_m . In the new version, this difference is now zero ($\delta\omega = 0$) beyond this level.

The evolution of the potential temperature difference ($\delta\theta$) between the inside and outside of cold pools is controlled by differential heating (δQ_1^{cv} , δQ_1^{wk}) due to deep convection and cold pools, as well as by damping due to gravity waves (τ_{gw}). The humidity difference (δq) follows a similar pattern, but without the damping effect of gravity waves. Heat sources are replaced by moisture sources (δQ_2^{cv} for convection and δQ_2^{wk} for cold pools).

$$\begin{cases} \partial_t \delta\theta = -\bar{\omega} \partial_p \delta\theta + \frac{\delta Q_1^{wk} + \delta Q_1^{cv}}{C_p} - \frac{K_{gw}}{\tau_{gw}} \delta\theta, \\ \partial_t \delta q = -\bar{\omega} \partial_p \delta q + \frac{\delta Q_2^{wk} + \delta Q_2^{cv}}{L_v}. \end{cases} \quad (1.2.6)$$

$$\text{où } \tau_{gw} = \frac{\sqrt{\sigma_{wk} - (1 - \sqrt{\sigma_{wk}})}}{4Nz\sqrt{D_{wk}}}$$

C_p is the heat capacity of dry air, N is the Brunt-Väisälä frequency, and z is altitude. K_{gw} is the efficiency of gravity waves. Finally, L_v is the latent heat of vaporization of water.

δQ_1^{wk} (respectively δQ_2^{wk}) depend on the entrainment (e_w) of dry air, the differential advection of $\bar{\theta}$ (respectively \bar{q}) and $\delta\theta$ (respectively δq). Similarly, δQ_1^{cv} (respectively δQ_2^{cv}) are influenced by heating trends associated with unsaturated currents ($Q_{cv}^{1,unsat}$, or $Q_{cv}^{2,unsat}$ for humidity) and saturated currents ($Q_{cv}^{1,sat}$, or $Q_{cv}^{2,sat}$ for humidity).

$$\begin{cases} \frac{\delta Q_1^{wk}}{C_p} = \frac{e_w}{\sigma_{wk}} \delta\theta - \delta\omega \partial_p \bar{\theta} - (1 - 2\sigma_{wk}) \delta\omega \partial_p \delta\theta \\ \frac{\delta Q_2^{wk}}{L_v} = \frac{e_w}{\sigma_{wk}} \delta q - \delta\omega \partial_p \bar{q} - (1 - 2\sigma_{wk}) \delta\omega \partial_p \delta q \\ \delta Q_1^{cv} = \frac{Q_{cv}^{1,unsat}}{\sigma_{wk}} - \frac{Q_{cv}^{1,sat}}{1 - \sigma_{wk}} \\ \delta Q_2^{cv} = \frac{Q_{cv}^{2,unsat}}{\sigma_{wk}} - \frac{Q_{cv}^{2,sat}}{1 - \sigma_{wk}} \end{cases}$$

Entrainment is determined from the vertical gradient of $\delta\omega$ and the cold pool spreading rate, according to the following relationship :

$$e_w = \sigma_{wk}(1 - \sigma_{wk}) \partial_p \delta\omega + \partial_t \sigma_{wk}$$

The equation 1.2.6, via the variables δQ_1^{cv} and δQ_2^{cv} , describes the impact of deep convection on cold pools which results in their cooling due to precipitating descents, as discussed above.

The cold pools model is now fully described. It includes :

- three prognostic variables, derived directly from the model equations : the profiles of $\delta\theta$ and δq and σ_{wk} .
- two diagnostic variables, evaluated from the profile of $\delta\theta$: C_* and WAPE
- two free parameters : the coefficient k and the density D_{wk}

~~On peut~~ On pourrait en mettre d'autres
 K_{gw} , T_{max}

Eq 1.2.8 Control of deep convection by cold pools

To take into account the effect of cold pools on convection, in particular the uplift at their gust fronts, the model introduces two new variables : the Available Lifting Energy (ALE_{wk}), involved in triggering convection, and an Available Lifting Power (ALP_{wk}), determining the intensity of convection.

To calculate ALE_{wk} , the model assumes that the maximum speed (C_{max}) on the cold pool contour will trigger convection. This is assumed to be proportional to the square root of $WAPE$, with a higher coefficient of proportionality here (arbitrarily estimated at 1), leading to the following relationship :

$$C_{max} = k' \sqrt{2WAPE} \quad (1.2.8)$$

where $k' = 1$

The Available Lifting Energy associated with cold pools is thus expressed by the following relationship :

$$ALE_{wk} = \frac{1}{2} C_{max}^2 \quad (1.2.9)$$

Combining equations (1.2.9) and (1.2.8) gives the expression for ALE_{wk} below :

$$ALE_{wk} = k'^2 WAPE \quad (1.2.10)$$

With $k' = 1$, this equation says that, in the cold pools model, the Available Lifting Energy associated with cold pools is equal to the collapse energy.

ALP_{wk} is calculated by assuming that cold pools exert a horizontal power on the surrounding air during its spreading. This horizontal power is then converted into vertical power. During this conversion, the model assumes that a large part of the horizontal power is dissipated, and that only 25% contributes to increasing the intensity of convection.

Each cold pool generates its own lifting power, depending on its spreading speed (C_*), height (h_{wk}) and the length (L_g) of its gust front. To obtain the average of these heavy powers, noted ALP_{wk} , we multiply the power of a cold pool by the den-

sity (D_{wk}) of cold pools. This leads to the following equation :

$$ALP_{wk} = \epsilon \frac{1}{2} \rho C_*^3 h_{wk} L_g D_{wk} \quad (1.2.11)$$

where $\epsilon = 0.25$ is the lifting efficiency with

Since L_g is not a variable in the cold pools model, we express ALP_{wk} as a function of σ_{wk} using the relations :

$$L_g = 2\pi r \quad (1.2.12)$$

$$\sigma_{wk} = D_{wk} \pi r^2 \quad (1.2.13)$$

The equations (1.2.12) and (1.2.13) allow us to express ALP_{wk} as a function of σ_{wk} by the relation :

$$ALP_{wk} = \epsilon \rho C_*^3 h_{wk} \sqrt{\sigma_{wk} D_{wk} \pi} \quad (1.2.14)$$

1.2.3 Large Eddy Simulations : LES

Large Eddy Simulations (LES) are numerical tools for simulating atmospheric phenomena with a horizontal resolution of tens to hundreds of meters. They are particularly well suited to the study of the thermodynamic structure of the boundary layer, as they resolve the eddies that form there. They offer an explicit and detailed representation of turbulent and convective movements within the boundary layer and associated clouds (Brown et al., 2002; Siebesma et al., 2003). While they are able to reproduce atmospheric thermodynamics and structure satisfactorily, the representation of cloud characteristics remains more delicate. They enable fairly direct simulation of turbulent and convective movements. In the presence of water phase changes, however, these simulations can become highly dependent on the microphysical schemes used. One of the major strengths of LES lies in its ability to provide three-dimensional information not available from observations, making it an indispensable complement to the latter for understanding processes. In addition, LES can be used to validate the internal variables of parametrizations, enabling their physical

Here

realism to be assessed. They have been ~~not~~ used to evaluate boundary layer and convection parameterizations (Rio et al., 2010; Couvreux et al., 2010). In recent years, they are increasingly used to document the characteristics of cold pools and guide their parameterization (Tompkins, 2001; Khairoutdinov and Randall, 2006; Couvreux et al., 2012; Feng et al., 2015).

In this study, we use the outputs of two oceanic LES and one continental LES. Both oceanic LES were carried out in Radiative-Convective Equilibrium (RCE) mode. RCE is a concept in which equilibrium is achieved between convective heating and radiative cooling of the atmosphere. In the RCE simulations used here, radiative fluxes are replaced by a constant cooling of -1.5 K per day, while the surface temperature is imposed. The destabilization leads to convection. The associated heating rate, largely corresponding to the release of latent heat, compensates for the cooling once quasi-equilibrium has been reached. For the two oceanic LES in RCE used here, one is performed with the SAM model (Khairoutdinov and Randall, 2003) and the other with MesoNH (Lac et al. 2018). Both simulations cover an oceanic domain of $200 \text{ km} \times 200 \text{ km}$ with horizontal resolution of 250 m, and the lateral boundary conditions are cyclic for both models. The sea surface temperature is set at 300 K. These two RCE ~~ocean~~ simulations run for 44 days, with equilibrium reached on simulation day 40. Output frequency for LES SAM is set to every 3 hours, while that for LES MesoNH is set to every 24 hours.

The continental LES is based on the AMMA (African Monsoon Multidisciplinary Analysis) case. This case is derived from observations made on July 10, 2006 during the AMMA field campaign (Redelsperger et al. 2006), during which a relatively small, short-lived convective system formed over Niamey (Lothon et al. 2011). This system, with a lifetime of around 6 hours, was observed by various instruments (radar and atmospheric soundings), supplemented by satellite data. This case study represents a typical example of deep convection in the Sahel regions. LES for this continental case is carried out with the MesoNH model over a $100 \text{ km} \times 100 \text{ km}$ domain, with a horizontal resolution of 200m. Lateral boundary conditions are cyclic and surface fluxes are imposed. Outputs are generated at a frequency of 10 minutes.

1.2.4 High-Tune Explorer (HTExplo) tool

General circulation models, used for global warming projections, are essentially based on a separation between the dynamical core, which manages large-scale air movements, and the physical parameterizations, enabling the impact of subgrid processes on the large scale to be represented. Progress in improving these models has

been slow in recent years, not only because of the difficulties of integrating these processes into the parameterizations, but also because of the complex tuning of the many free parameters involved in their formulation. This is the background to the development of the High-Tune Explorer (HTExplo) tool.

HTExplo has been developed in collaboration between the LMD (Paris), the Centre National de Recherche Météorologiques (CNRM/Météo-France) and the University of Exeter (UK). It is an automatic calibration tool for free parameters, based on machine learning techniques from the uncertainty quantification community (Williamson et al., 2013). This approach proposes a new calibration paradigm : instead of optimizing parameter values, it aims to identify the subset of parameters that enables the model to reproduce certain observables to a certain accuracy. The main steps involved in using the tool, as well as its mathematical foundations, are well described in Couvreux et al. (2021). The HTExplo tool was used for the first time in a SCM/LES comparison on several boundary layer cases of the LMDZ model, in order to characterize the subspace of free parameter values for which SCM simulations are consistent with LES for certain metrics and a given tolerance (Couvreur et al. 2021). This information was then used by Hourdin et al (2021) to calibrate the 3D configuration. These authors demonstrated how reducing the parameter space using this method significantly saves computing resources and reduces the time-consuming manual model tuning phase. They also pointed out that this approach eases the burden on the modeler, enabling him or her to concentrate more on understanding and improving the physical parameterizations of the model.

1.3 Analysis of cold pools in the LES

~~In this results section, we analyze the operation of cold pools based on LES and verify some of the equations internal to the parametrization.~~

1.3.1 Sampling

In order to use LES to study and modeling cold pools, the first challenge is to separate cold pools from their environment. Indeed, there is no a priori established framework for objectively identifying cold pools in observations and numerical models (Rochetin et al. 2021), and choices may depend in part on the physical picture one has of cold pools, and also, for the purpose at hand, on the picture underlying the parameterization. The first method for identifying cold pools proposed by Young

et al. (1995) was based on surface precipitation rates. In more recent studies, such as those by Provod et al. (2016); Zuidema et al. (2017); Vogel et al. (2021); Rochetin et al. (2021); Touzé-Peiffer et al. (2022), the detection of cold pools is closer to a density current oriented detection, in which variations in temperature, pressure and wind are taken into account. In the cases presented here, however, the boundary conditions are idealized so as to approximate the statistical stationarity assumptions underlying the decomposition between dynamic ^{core} ~~kernel~~ and parameterizations. Because of this homogeneity, cold pools can be identified fairly immediately and partly independently of these choices. In these cases, they can be easily detected from the anomaly of temperature at 10 m (T_{10m}), since surface temperatures are uniform. It should also be noted that, unlike other studies, the aim here is not to isolate individual “cold pools objects”, but only to know if we are inside or outside a cold pool. Here, cold pools are simply identified as the part of the domain where the anomaly of temperature at 10 m is below a threshold.

The map of divergence of wind at 10 m, smoothed on a $3.25 \text{ km} \times 3.25 \text{ km}$ box, enables us to visually identify centers and gusts fronts of cold pools, represented respectively by the maximum and minimum of divergence of wind at 10 m (Fig. 1.2 and Fig. 1.3). We superimpose on this map T_{10m} anomaly contours with different values to determine an optimal threshold for this anomaly. This optimal threshold corresponds to the value of the T_{10m} anomaly contour that surrounds cold pools centers and better follows gust fronts. Maxima of divergence of surface wind indicate the center of cold pools where cold air masses collapse. Precipitation is generally co-located with these divergence maxima. The fairly strong wind convergence observed around cold pools centers corresponds to the strong lift of air masses created upstream of the gust front at the cold pool's periphery.

Both the LES in RCE and the LES in the AMMA case show cold pools groupings (or very close cold pools centers) forming a common gust front. This can be explained by the fact that, during propagation, cold pools can merge to create a single, larger cold pools. We can also observe that wind convergence is generally more intense between the centers of grouped cold pools, indicating that updrafts of air masses associated with gust fronts is more pronounced when these cold pools meet. This is in line with some studies that indicate that convection initiation on gust fronts is more efficient when two or more cold pools collide (Mayer and Haerter, 2020; Torri, and Kuand, 2019; Haerter and Schlemmer, 2018; Feng et al, 2015). To set the T_{10m} anomaly values, the distinct characteristics of the ocean and continental cold pools were taken into account. The T_{10m} anomaly values used are higher on the RCE case

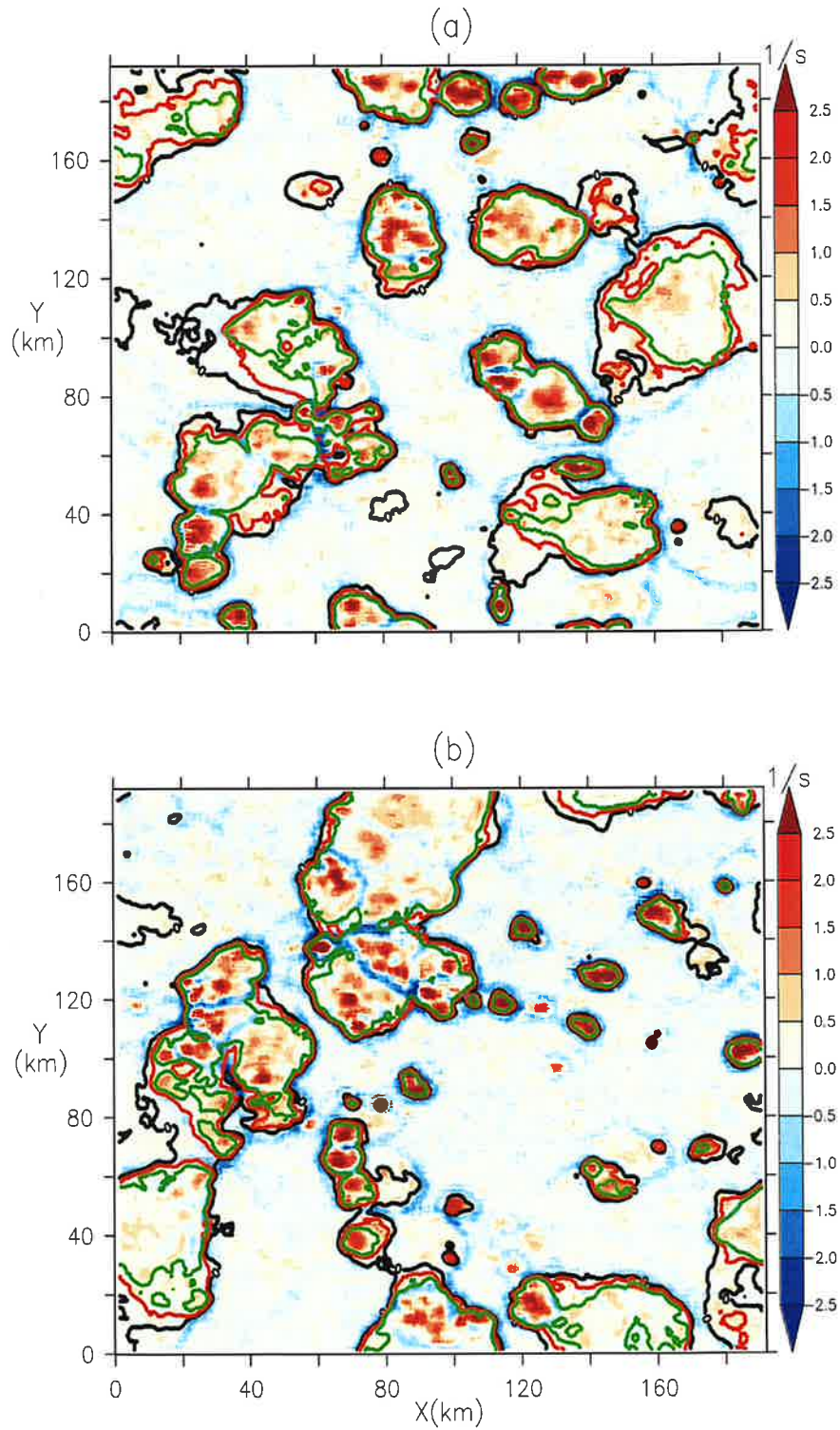


FIGURE 1.2 – Map of divergence of wind at 10 m (in s^{-1}) multiplied by 1000 and smoothed horizontally over $3.25 \text{ km} \times 3.25 \text{ km}$ represented on two instants (a and b) of the LES SAM carried out on the oceanic RCE case and superimposed with the contours of temperature anomalies at 10 m at -0.4 K (green), -0.2 K (red) and 0 K (black).

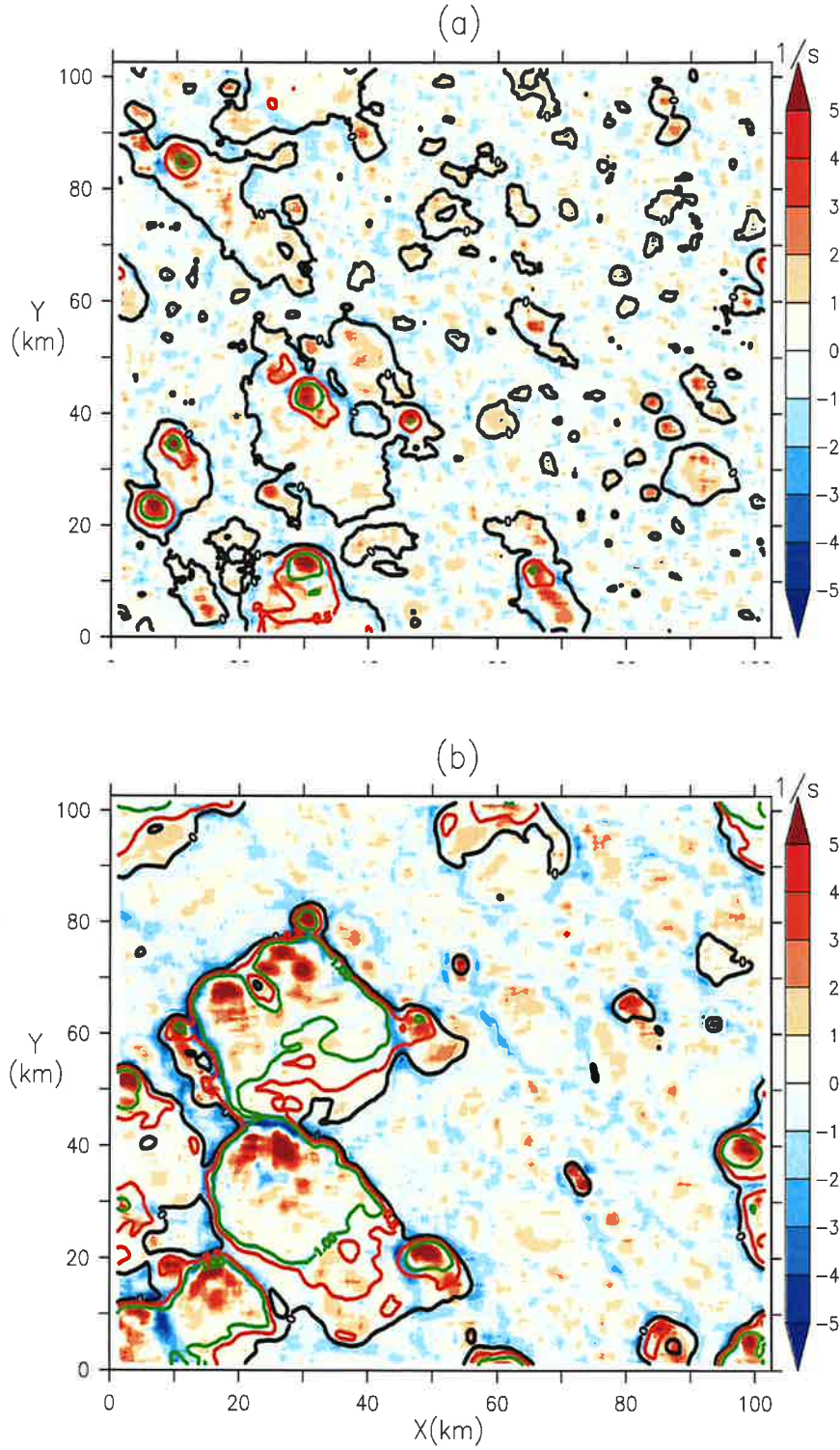


FIGURE 1.3 – Map of divergence of wind at 10 m (in s^{-1}) multiplied by 1000 and smoothed horizontally over $3.25 \text{ km} \times 3.25 \text{ km}$ represented on the 17 :10 (a) and 18 :00 (b) instants of the LES MESONH carried out on the AMMA case and superimposed with the contours of anomalies of temperature at 10 m at -1 K (green), -0.5 K (red) and 0 K (black).

(0 K, -0.2 K and -0.4 K) and slightly lower on the AMMA case (0 K, -0.5 K and -1 K), as the cold pools there are colder. In the RCE case, the T_{10m} anomaly at 0 K sometimes includes regions without cold pools centers, where divergence of surface wind is low (Fig 1.2a and 1.2b). This suggests that the threshold may be too high to accurately identify cold pools in this case. Figures 1.2a and 1.2b also show that T_{10m} anomaly contours with thresholds of -0.2 K and -0.4 K surround the centers of cold pools quite well, but those with a threshold of -0.2 K follow the edges of cold pools better. In the case of AMMA, figure 1.3a clearly shows that the 0 K threshold is too high to identify cold pools. Figure 1.3b, on the other hand, shows that the -1 K threshold follows gust fronts of cold pools better than the -0.5 K threshold. On the basis of these analyses, we retain the T_{10m} anomaly thresholds at -0.2 K and -1 K to identify cold pools in the RCE and AMMA cases respectively.

sampling of cold pools : after selecting values for the T_{10m} anomaly to separate the inside and outside of cold pools in the RCE and AMMA cases, we carry out sampling to calculate certain variables of cold pools model in the LES. We first determine the vertical profiles of temperature (δT), humidity (δq) and vertical velocity (δw) differences between inside and outside of cold pools. To do this, we apply a mask calculated from the temperature at 10m threshold identified earlier. This is applied to the entire column to determine the vertical profiles. This vision of vertical cylinders is obviously open to question. But it does seem to apply, at least to the cases studied here. The deviations δX are obtained as the difference between the average profile of the variable X inside cold pools and the average profile outside.

Calculating Available Lifting Energy and Power : we calculate the variables of Available Lifting Energy (ALE_{wk}) and Power (ALP_{wk}) associated with cold pools in the LES. To do this, we proceed in several steps :

1. We determine an average cloud-base height at which we calculate the $w_b(x, y)$ (vertical velocities at cloud base). This height corresponds to the altitude at which the average profile of condensed water reaches its first non-zero value. It is observed at around 950 hPa on the two oceanic LES (SAM and MesoNH) and at around 750 hPa on the LES for the AMMA case (MESONH) (Fig. 1.4). The w_b on the RCE case and on the AMMA case therefore correspond respectively to vertical velocities located on the 950 hPa and 750 hPa levels.
2. We create a mask for gust fronts of cold pools based on the $w_b(x, y)$ values computed for each point of the LES horizontal grid. Since the updrafts on gust fronts are both stronger and more coherent horizontally than the thermals observed in the environment of cold pools, we used ~~both~~ threshold of ~~$w_b(x, y)$~~

①
the
②
③
① suff.
Si c'est
"premier"
"non-zero"
après ça le
point moyen
le plus bas
du domaine.

après a

On line 1 above it is just to send inside, non ?

and horizontal smoothing over $1.25 \text{ km} \times 1.25 \text{ km}$ (RCE) et $2 \text{ km} \times 2 \text{ km}$ (AMMA) to define this mask. The smoothed w_b values are denoted as $\tilde{w}_b(x, y)$ in the rest of the text. After several analyses, we selected $\tilde{w}_b(x, y)$ thresholds of 0.6 m/s for the RCE case and 2 m/s for the AMMA case to identify gust fronts.

3. We distinguish the updrafts on gust fronts from those associated with thermals. The updrafts on gust fronts are defined by the $w_b(x, y)$ values within the gust fronts mask, while those due to thermals correspond to the $w_b(x, y)$ values located outside this mask.

Figure 1.5 presents maps of T_{10m} anomaly, smoothed horizontally on a $2.5 \text{ km} \times 2.5 \text{ km}$ grid, for the RCE and AMMA cases. On these maps, we have overlaid the contours of the T_{10m} anomalies used to identify cold pools (-0.2 K for RCE and -1 K for AMMA), as well as the updrafts on gust fronts (in red) and thermals (in green). Visually, the gust fronts computed with $\tilde{w}_b(x, y)$ thresholds of 0.6 m/s (RCE) and 2 m/s (AMMA) align well with the contours of cold pools identified using these T_{10m} anomaly thresholds. It also appears that most thermals are located in the environment of cold pools for both the RCE and AMMA cases (Fig. 1.5). This retrospectively validates a choice made in version 6A of the model, where the effect of thermals was only computed outside cold pools.

Finally, to determine ALE_{wk} , we take the maximum kinetic energy in the domain, considering only $w_b(x, y)$ in the gust fronts mask ($w_{bgust}(x, y)$), as it is the maximum vertical velocity on the gust front that triggers convection. As for ALP_{wk} , which represents the average updrafts power provided by all cold pools in the domain, it is calculated from the horizontal average of the cube of w_{bgust} , weighted by the surface fraction (σ_{gust}) covered by gust fronts. The mask applied to gust fronts was used to calculate σ_{gust} , which is 0.017 for the RCE case and 0.067 for the AMMA case, for the times shown in figure. 1.5.

$$ALE_{wk} = \max\left(\frac{1}{2}w_{bgust}^2\right) \quad (1.3.1)$$

$$ALP_{wk} = \sigma_{gust} \frac{1}{2} \overline{\rho w_{bgust}^3} \quad (1.3.2)$$

Calculation of the spreading speed, C_* : we assume, as in the parametrization, that cold pools are identical disks of the same radius (r). This assumption makes

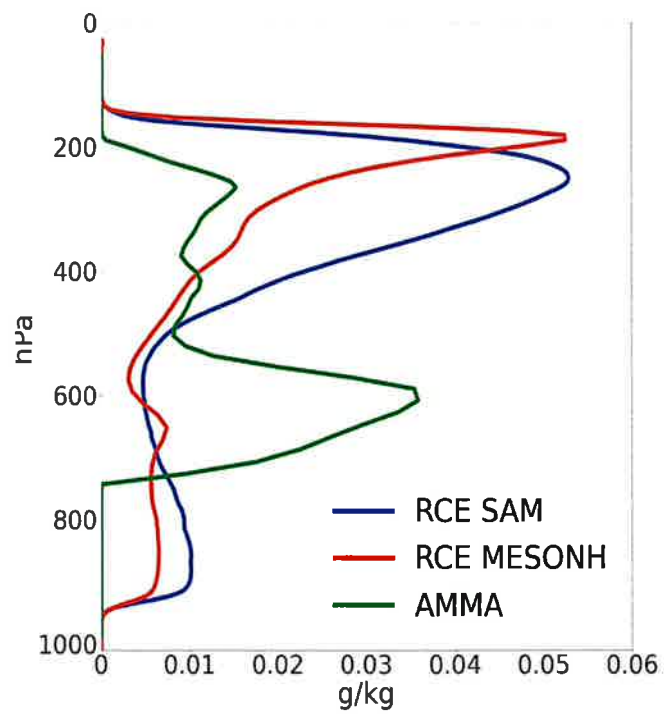


FIGURE 1.4 – Vertical profile of condensed water averaged horizontally on the LES in oceanic RCE carried out with the SAM and MésNH models and the continental LES of the AMMA case carried out with MésNH.

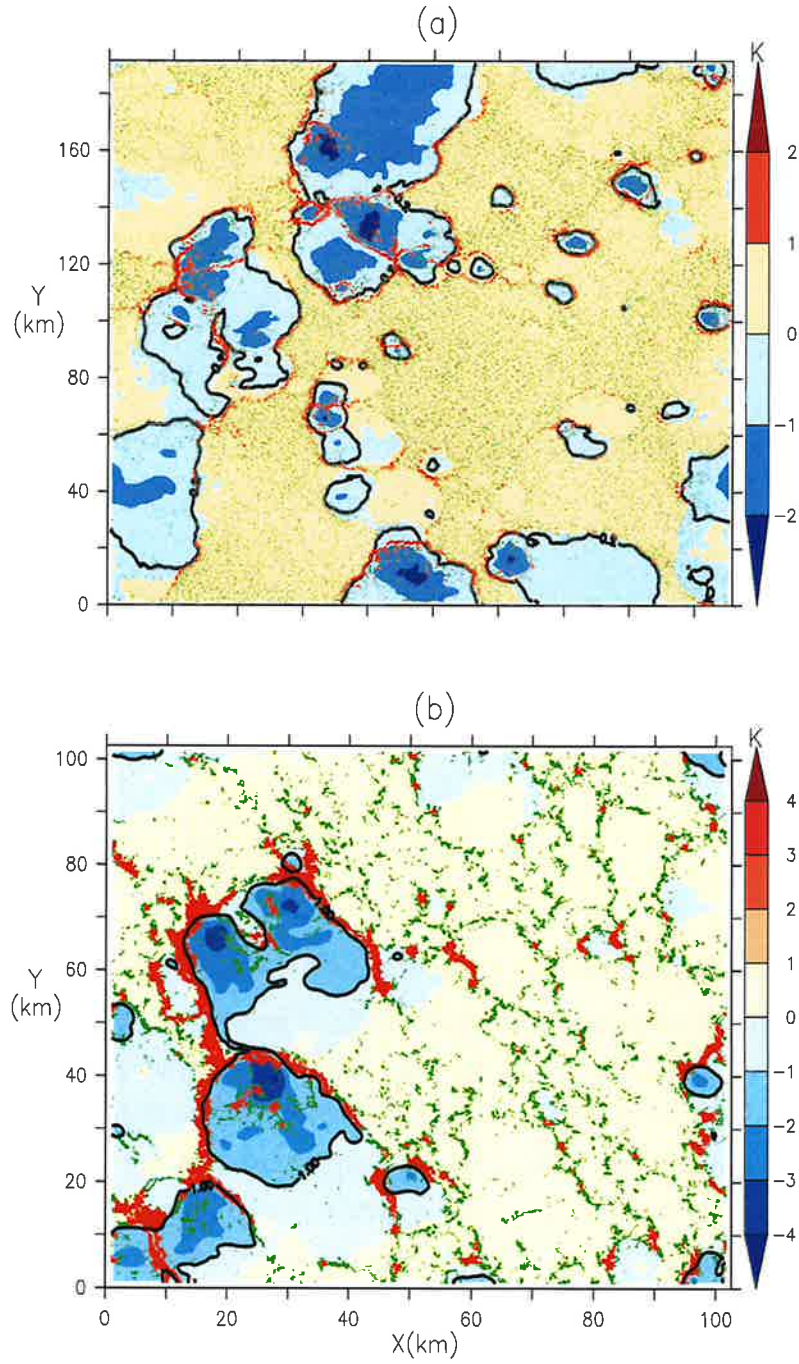


FIGURE 1.5 – Maps of anomaly of temperature at 10 m, smoothed horizontally over $2.5 \text{ km} \times 2.5 \text{ km}$, represented on an instant of the LES SAM of the RCE case (a) and on the instant 6 :00 PM of the LES of the AMMA case with black contours indicating thresholds of temperature at 10 m anomaly of -0.2 K (RCE) and -1 K (AMMA). The red color indicates the updrafts on the gust fronts given by the vertical velocities at cloud base (w_b) in the gust fronts mask, which is determined by the w_b smoothed horizontally over $1.25 \text{ km} \times 1.25 \text{ km}$ and exceeding 0.6 m/s (RCE) and over $2 \text{ km} \times 2 \text{ km}$ with a value greater than 2 m/s (AMMA). The green dots represent thermals, defined by w_b outside the gust front mask.

it easy to determine C_* by of the divergence theorem, which asserts the equality between the integral of the diverging wind on the surface of cold pools and the flux of this wind across the edges of cold pools.

$$\int \int \text{div}(\vec{V}_{10}) dS_{wk} = C_* L_g \quad (1.3.3)$$

$$C_* = \frac{\overline{\text{div}(\vec{V}_{10}) S_{wk}}}{L_g} \quad (1.3.4)$$

where S_{wk} is the surface of cold pools

$$S_{wk} = \pi r^2 \quad (1.3.5)$$

The equations 1.2.12, 1.2.13 and 1.3.5 allow us to express C_* as a function of the mean divergence of wind at 10 m, the surface fraction (σ_{wk}) and the density (D_{wk}) of cold pools by the relation :

$$C_* = \frac{1}{2} \overline{\text{div}(\vec{V}_{10m})} \sqrt{\frac{\sigma_{wk}}{D_{wk} \pi}} \quad (1.3.6)$$

To apply this calculation of C_* in the LES, we take the horizontal average of the surface wind divergence inside cold pools. The surface fraction (σ_{wk}) of cold pools calculated in the LES is 0.12 for the AMMA case and 0.25 for the RCE case. To determine D_{wk} , we manually counted the centers of cold pools visible on the surface wind divergence maps (Fig. 1.2 and 1.3), as we did not use automated detection methods in this study that could generate their number automatically. We find an approximate density, D_{wk} , of 5 cold pools per $100\text{km} \times 100\text{km}$ for both the RCE and AMMA cases

Calculation of collapse energy : we finally calculate the collapse energy (W_{APE}) of cold pools in the LES using equation (1.2.2) proposed by Grandpeix et al. (2010). The task consists of determining $\overline{\theta_v}$, as well as the profiles of $\delta\theta_v$ and h_{wk} in the LES. To do this, we first computed δT in the LES, then derived $\overline{\theta_v}$ and the profile of $\delta\theta_v$. Regarding the determination of h_{wk} , as suggested by Grandpeix et al. (2010), we take this height at the altitude where the δT profile cancels out. This altitude is around 950 hPa (approximately 600 m) in the oceanic RCE case and around 800 hPa (approximately 2 km) in the AMMA case (Fig. 1.6).

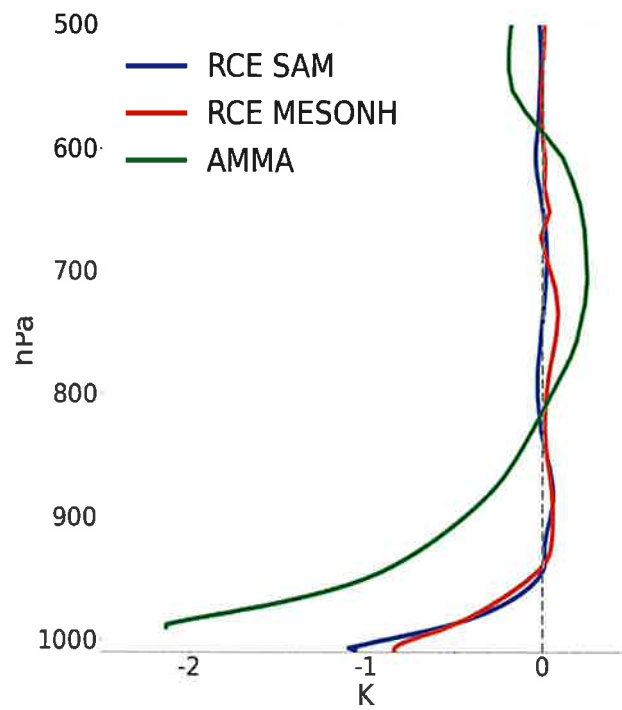


FIGURE 1.6 – Vertical profiles of the temperature difference between the inside and the outside of cold pools calculated at an instant of the LES (SAM and MESONH) of the RCE case and an instant of the LES MESONH of the AMMA case.

1.3.2 Validation of Phenomenological Laws

Physical parameterizations are defined by sets of mathematical equations intended to represent the subgrid process within a column of the model. The formulation of these equations is based both on a phenomenological understanding of the processes concerned and on fundamental principles of physics. These parameterizations can be validated in bulk, or piecewise, by isolating certain equations or relations between internal variables, or between internal variables and state variables of the GCM. LES offer the possibility of performing a priori validation and adjustment of these laws.

In the cold pools model, variables ALE_{wk} , ALP_{wk} and C_* are determined from the collapse energy ($WAPE$) (see equations (1.2.1), (1.2.10) and (1.2.14)), based on assumptions derived from physical laws. In this section, we verify the validity of calculations of ALE_{wk} , ALP_{wk} and C_* based on $WAPE$, as well as the underlying physical assumptions, based on the LES. To do this, we first recalculate these three variables in the LES using the $WAPE$ from the sampled $\delta\theta_v$ profiles, with the formulas of the parameterization. For D_{wk} , σ_{wk} and h_{wk} in the calculation of ALP_{wk} (equation (1.2.14)), we also take the values estimated in the LES. We then compare the recalculated values of ALE_{wk} , ALP_{wk} and C_* from the $WAPE$ with those obtained in the LES, derived from the vertical speed at the cloud base near the gust fronts (w_{bgust}) for ALE_{wk} and ALP_{wk} , and from the mean divergence of wind at 10 m in cold pools for C_* .

Table 1.1 shows that, for the LES of the RCE case made with MesoNH and the AMMA case, the values of ALE_{wk} calculated from w_{bgust} and $WAPE$ from the $\delta\theta_v$ profiles are very close. In the LES of the RCE case made with SAM, ALE_{wk} calculated from w_{bgust} is slightly higher than the $WAPE$ from the $\delta\theta_v$ profile (table 1.1). However, even in this case, ALE_{wk} determined from w_{bgust} remains comparable to the $WAPE$ derived from the $\delta\theta_v$ profile. These results for the three LES validate the hypothesis of equality between ALE_{wk} and $WAPE$, as estimated by the parameterization.

As for C_* , table 1.1 shows that, for the three LES, its values calculated from the $WAPE$ are systematically lower than those allowed from the mean divergence of wind at 10 m in cold pools. This difference could be due to an underestimation of the coefficient k , imposed here at 0.33. By setting k to 0.66, the calculation of C_* based on the $WAPE$ becomes comparable to those obtained from the mean divergence of wind at 10 m in cold pools, notably for the RCE and AMMA cases (table 1.1).

TABLE 1.1 – Comparison of the variables of $WAPE$, ALE_{wk} , C_* and ALP_{wk} calculated in the samplings (E) and those calculated with the formulas of the parameterization (FP) for the coefficient $k = 0.33$ and $k = 0.66$ in the oceanic LES in RCE carried out with SAM and MESONH and in the continental LES of the AMMA case carried out with MESONH

	$WAPE$ (J/Kg)	ALE_{wk} (J/kg) (E)	C_* (m/s) (FP) $k=0.33$	C_* (m/s) (E)	C_* (m/s) (FP) $k=0.66$	ALP_{wk} (J/kg) (FP) $k=0.33$	ALP_{wk} (J/kg) (E)	ALP_{wk} (J/kg) (FP) $k=0.66$
RCE SAM	7.962	10.460	1.315	2.228	2.630	0.008	0.054	0.071
RCE MESO	7.912	6.965	1.313	2.264	2.625	0.008	0.020	0.071
AMMA MESO	34.250	33.480	2.727	4.939	5.454	0.104	0.982	0.831

As discussed above, the value of 0.33 was retained following an oral communication by Lafore (2000). But other studies propose different values : Lafore and Moncrieff (1989) estimate k at 0.68 based on CRM simulations of 2D grain lines, while Bryan et al. (2005) estimate it at 0.5 from observations of cold pools during the BAMEX experiment in the American Great Plains. These results would also validate the hypothesis of the model which postulates that the kinetic energy of cold pools results from the transformation of $WAPE$ into kinetic energy with a coefficient k compatible with the published estimates.

As for ALP_{wk} , the table 1.1 shows that, for the three LES, its values calculated with C_* from the $WAPE$ are much lower than those obtained from the w_{bgust} sampled in the LES. We observe a difference of at least a factor of 3 between the two sets of values of ALP_{wk} for both the two LES of the RCE case and for the LES of the AMMA case. Two coefficients are involved in the calculation of ALP_{wk} with the parameterization formula : the coefficient k and the lifting efficiency ϵ , imposed respectively at 0.33 and 0.25. The low values of ALP_{wk} obtained could therefore be due to the choice of the values of these parameters, set relatively arbitrarily until now. To check this, we recalculate ALP_{wk} with the parameterization formula taking $k = 0.66$ in the calculation of C_* , as suggested by the previous analyses. Comparisons made on the three LES show that the values of ALP_{wk} thus recalculated are clearly closer to the values of w_{bgust} obtained by sampling (table 1.1). Having the right values of ALP_{wk} with the parameterization formula for the LES of the RCE and AMMA cases, simply by adjusting C_* with $k = 0.66$, justifies the calculation of ALP_{wk} for these two cases. This also allows to estimate ϵ at 0.25 for these two cases,

allows to reconcile the two estimates.

~~This~~ which is compatible with the hypothesis of the parameterization according to which 25% of the horizontal power provided by the cold pools during its propagation would be used to reinforce the intensity of the convection while a large part dissipates.

1.4 Comparison between LES and standard LMDZ

1.4.1 The profiles of δT , δq and δw

In this section, we evaluate the profiles of δT , δq and δw computed in LES versus those simulated with LMDZ. The comparison is more demanding than those shown in the previous section since all parameterizations interact with each other to arrive at the simulated values several hours (AMMA) or days (RCE) after initialization. ~~We begin with a description of the method used to perform these comparisons.~~ For LES in RCE, we represent the profiles once a quasi-steady state has been reached. It is this quasi-steady state that the convective radiative equilibrium framework targets. Regarding the LES of the AMMA case, intermediate analyses show that cold pools appear in the afternoon around 5 :00 PM with relatively low temperatures and develop during the day. Due to the variations in cold pools characteristics at different times on the continent, we average the results over the 7 available times between 5 :00 PM and 6 :00 PM to simplify our analyses. To compare with the model, we perform a single-column LMDZ control simulation (LMDZ CTRL) for the RCE and AMMA cases. These LMDZ simulations are performed with exactly the same initial and boundary conditions as the corresponding LES. For the RCE case, we perform a 44-day LMDZ CTRL simulation to reach a quasi-equilibrium. For the AMMA case, the LMDZ CTRL simulations are performed over the day of July 10, 2006, from 6 :00 AM to midnight.

Trig. Conf. For the AMMA case, the cloud size threshold controlling the triggering of deep convection is adjusted so that convection triggers at the same time as in the LES in order to allow a precise comparison. Indeed, convection triggers before 2 :00 PM in the AMMA case with the standard LMDZ configuration, while in the LES, it appears around 5 :00 PM. To obtain a triggering simultaneous with that of the LES, we performed tests by modifying the threshold size from which a cumulus transforms into a cumulonimbus in the model. These tests made it possible to obtain the triggering of convection in the LMDZ simulation of the AMMA case at 4 :50 PM by setting this threshold at 24 km^2 . In order to facilitate comparisons between LMDZ and LES, we also impose in the LMDZ simulations the density of cold pools estimated in the LES. We thus set a density of 5 cold pools per $100\text{km} \times 100\text{km}$,

both for the RCE and AMMA cases. To represent the profiles of δT , δq and δw in LMDZ CTRL for the RCE case, we perform a time average between the 41st and 43rd day of simulation, in order to compare with the LES at the same times. For the AMMA case, we perform an average between 5 :00 PM and 6 :00 PM, as in the LES.

case with a surface anomaly about 3 times deeper in the AMMA than in the RCE case
~~Before starting this comparison, we perform a detailed analysis of the δT , δq and δw profiles in the LES. The analysis of the δT profiles in the LES shows that cold pools are colder at the surface with temperatures increasing towards the top both in the RCE case (Fig. 1.7a) and in the AMMA case (Fig. 1.7d). The δT profiles of the LES show that the cold pools temperatures are quite similar in these two cases, which seems to contradict the observations indicating colder cold pools on the continent. This could be explained by the fact that, in this continental case, we perform the analyses at the first moments after the appearance the cold pools, when they are not yet fully developed. This case also corresponded to relatively sporadic and local convection events. On the δq profiles, the LES show that cold pools are wetter at the surface in both the RCE and AMMA cases (Fig. 1.7b and Fig. 1.7e). This difference reverses towards the top of cold pools altitude at which the cold pools are dried by a subsidence of dry air masses (Fig. 1.7c and 1.7f). On the RCE case, this subsidence vanishes below 800 hPa (Fig. 1.7c), while for the AMMA case, it vanishes at a higher level, around 600 hPa (Fig. 1.7f).~~

Observed Cold pools are however often colder over continents
is consistent with
~~We now move on to the comparisons of the δT , δq and δw profiles simulated by LMDZ with those calculated in the LES. The δT profiles simulated with LMDZ CTRL show that the temperatures in cold pools are lower at the surface, increasing progressively towards the top, both in the RCE and AMMA cases (Fig. 1.7a and Fig. 1.7d), in coherence with the LES. These δT profiles in LMDZ CTRL cancel at the same altitude as those calculated in the LES for these two cases. We observe, however, that in the RCE case, cold pools are colder in the LES than in LMDZ CTRL (Fig. 1.7a), while for the AMMA case, cold pools are slightly colder at the surface in LMDZ CTRL than in the LES (Fig. 1.7d). The analysis of the δq profiles simulated with LMDZ CTRL also shows that in the RCE and AMMA cases, cold pools are wetter at the surface and that this humidity decreases towards the top (Fig. 1.7b and Fig. 1.7e), which is consistent with the LES. In both cases, cold pools are associated with subsidence. The height at which this subsidence of air masses vanishes is observed at higher pressure levels in the LES (below 800 hPa on the RCE case and below 600 hPa on the AMMA case) compared to LMDZ, where it is~~

are qualitatively consistent with LES
but with the variations of δq are on the vertical axis much larger than in the LES.

in the top of the pool is much to dry. close to dry. In ventilation, the cold pool is much to dry.

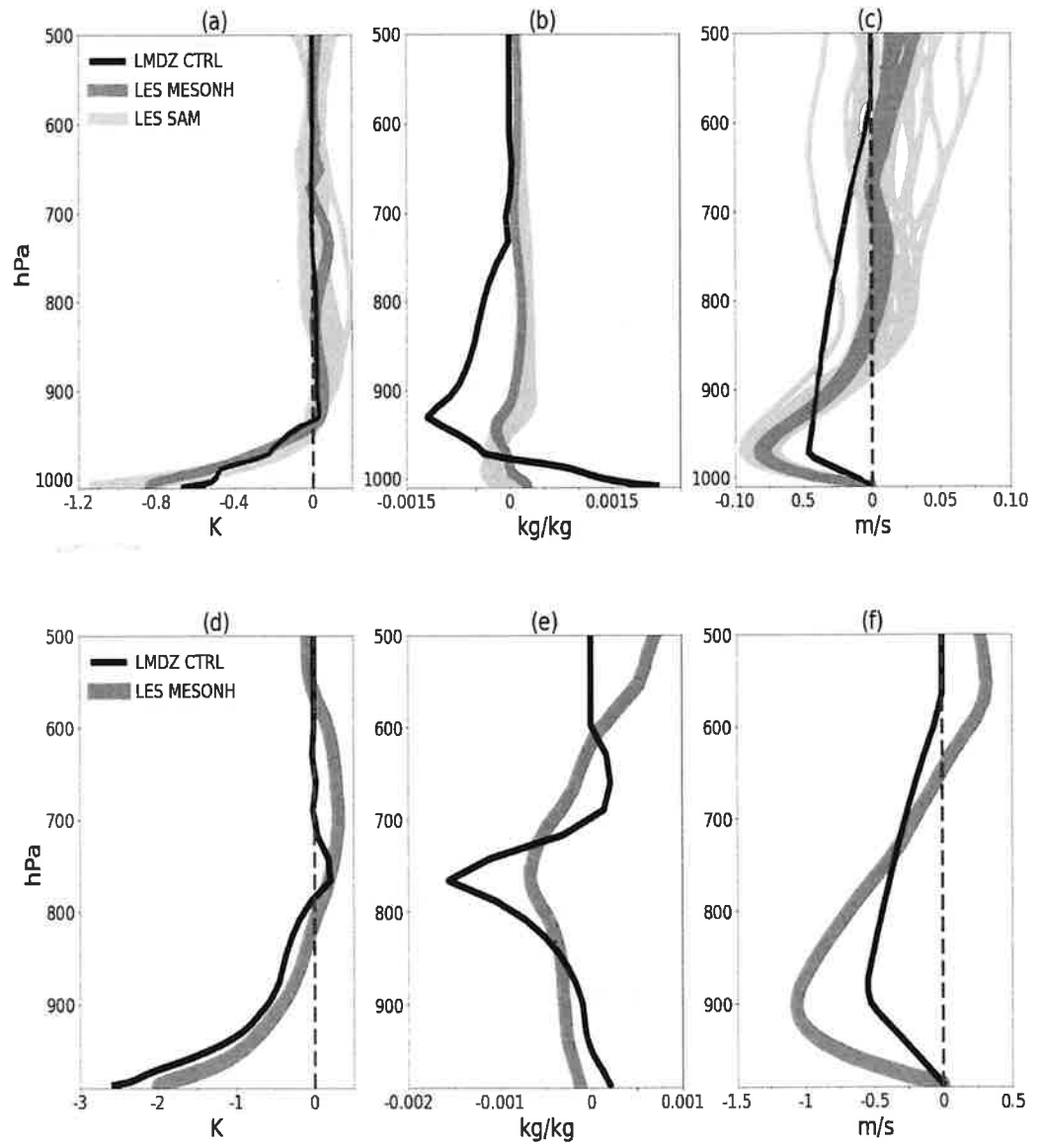


FIGURE 1.7 – Vertical profiles of δT , δq and δw calculated in the LES and simulated by LMDZ control (LMDZ CTRL) on the RCE case (a, b, c) and on the AMMA case (d, e, f).

This may clearly explain be responsible for the strong dry bias at h_{wp} and above.
 observed above h_m (fixed at 600 hPa) in both cases. We also find that cold pools are much too dry at the top in LMDZ CTRL compared to the LES, both on the RCE and AMMA cases (Fig. 1.7b and Fig. 1.7e). The comparisons also reveal that the model simulates wetter cold pools at the surface than those in the LES in both cases, with a more pronounced difference for the RCE case.

1.4.2 The variables $WAPE$, ALE_{wk} , C_* et ALP_{wk}

In this section, we compare the variables $WAPE$, ALE_{wk} , C_* and ALP_{wk} calculated in the LES with those simulated by LMDZ CTRL ~~for the RCE and AMMA cases~~. Like the vertical profiles, the results are averaged over the days following the achievement of equilibrium (days 41, 42 and 43) for RCE and over the available instants between 5 :00 PM and 6 :00 PM for AMMA.

Table 1.2 shows that, ~~for the RCE case~~, the $WAPE$ variable simulated by LMDZ CTRL is significantly lower than those of the LES SAM and the MésosNH, with a difference of at least a factor of 2. These low values of $WAPE$ in LMDZ CTRL also translate into low ALE_{wk} ~~compared to the LES SAM and the MésosNH~~ (table 1.2). *Values LES* Indeed, the ALE_{wk} on the RCE case are at least twice as low in LMDZ CTRL as in the LES. On the other hand, for the AMMA case, the $WAPE$ simulated by the model are globally in agreement with the values calculated in the LES (table 1.2), which allows the model to obtain ALE_{wk} comparable to those of the LES for this case (table 1.2). As for C_* , the comparisons between the values simulated by LMDZ CTRL and those calculated in the LES show that the values in LMDZ CTRL are at least twice as low, both for the RCE case and for the AMMA case (table 1.2). As for ALP_{wk} , the values simulated by LMDZ CTRL are significantly lower than those of the LES for both cases, with a difference of at least a factor of 10 (table 1.2).

In summary, the comparisons with the LES carried out on the oceanic RCE case and the AMMA case highlight the difficulties of the model in reproducing the humidity of cold pools for both cases, as well as the temperature of cold pools for the RCE case.

1.5 Improvements of cold pools model

Here, we test different modifications to improve the representation of temperature and humidity in the cold pools model. We start by correcting the observed

TABLE 1.2 – Comparison of the variables $W A P E$, $A L E_{w k}$, C_* and $A L P_{w k}$ calculated in the LES from the samples and simulated by LMDZ control (LMDZ CTRL) on the oceanic case in RCE and the continental case (AMMA)

	$W A P E$ (J/Kg)	$A L E_{w k}$ (J/kg)	C_* (m/s)	$A L P_{w k}$ (J/kg)
RCE				
LES SAM	7.962	10.460	2.228	0.054
LES MESONH	7.912	6.965	2.264	0.020
LMDZ CTRL	2.957	2.957	0.802	0.001
AMMA				
LES MESONH	34.250	33.480	4.939	0.982
LMDZ CTRL	30.430	30.430	2.574	0.042

discrepancies between the LES and the model concerning the value of the coefficient k and the altitude h_m , in order to assess their impact on the variation of temperature and humidity, before exploring other avenues.

1.5.1 Coefficient k

We start by testing in LMDZ the impact of taking a value of 0.66 rather than 0.33 (LMDZ V1), as suggested by the LES. We analyze the effect of this change on the δq and δT profiles of the model. Simulations of LMDZ V1 show that changing to a value of 0.66 for the k coefficient results in slight changes in the δq and δT profiles, for the RCE and AMMA cases (Fig. 1.8). However, we observe that, even with the modification of k to 0.66, cold pools still remain too dry at the top and wetter at the surface compared to the LES on both cases (Fig. 1.8b and Fig. 1.8e). Concerning temperatures, in the RCE case, cold pools also remain always less cold in LMDZ MODIF1 than in the LES (Fig. 1.8a). On the other hand, in the AMMA case, we observe that the passage from k to 0.66 leads to a slight flattening of the δT profile, which nevertheless always remains close to the LES results (Fig. 1.8d). These analyses show that the impact of this change on the humidity and temperature variations of cold pools is globally low.

1.5.2 Altitude h_m

In the previous sections, we found that the altitude at which the subsidence of dry air masses in cold pools vanishes is observed in LES below 800 hPa for the RCE case and below 600 hPa for the AMMA case, while in LMDZ, this altitude h_m was arbitrarily set to 600 hPa in the original version of the parameterization.

In this section, we made the value of h_m dependent on the height (h_{wk}) of cold

→ In version V2, we compute h_m as αh_{wk} where $\alpha \approx 0.8$ (to be considered as a new free parameter in the following section)

~~also~~
~~pools in order to approximate the LES results. First, note that we took the mass flux of the convective current above h_m to be zero. This allows us to consider only the lateral entrainment of air in cold pools, which now vanishes at h_m . Intermediate tests showed that this change has almost no impact on the results. We then adjust h_m . Since this altitude is observed in the LES at different levels for the two cases, we calculate it as a function of the height (h_{wk}) of the top of cold pools in order to account for this regional variation in the model. Thus, to better match the LES, we set h_m to a height that is equal to approximately three times (this factor can become an adjustable parameter of the model) the altitude of cold pools top in both the RCE and AMMA cases. We then perform a simulation of LMDZ with this new formulation of h_m , also integrating the modification of the coefficient k (LMDZ V2). Comparisons between LMDZ V2 simulations and LES show a better representation of the δq profile at the top of cold pools in both the RCE and AMMA cases (Fig. 1.8b and Fig. 1.8e). These results show that the too low humidities simulated at the top of cold pools with LMDZ CTRL are due to h_m which is imposed at a level that is much too high in the initial parameterization compared to the LES. This increases the supply of dry air into the cold pool, drying the air at the top. The fact that the model is able to reproduce the humidity at the top of cold pools as in the LES by just adjusting h_m validates the physics implemented in this cold pools scheme. This reveals that a limitation of this scheme lay in the choice of the value of a parameter (the height above 600 hPa) rather than in the formulation themselves. If this modification reduces the humidity at the surface of cold pools in the RCE case, we nevertheless observe that cold pools always remain more humid at the surface in the model than in the LES. As for the δT profiles, the figures (Fig. 1.8a and Fig. 1.8d) indicate that this modification has no impact on the δT profiles in the AMMA case, but that it very slightly increases temperatures of cold pools in the RCE case.~~

1.5.3 The tuning

In this section, we focus mainly on improving the representation of the profile of δT for the RCE case compared to the LES, given that the two previous modifications had a very limited impact on this profile. Thus, we use the HTEExplorer tool to fit the δT profile of the model to LES. To do this, we simultaneously explored several model parameters by assigning them wide ranges of possible values in order to identify those that have an influence on the temperature of cold pools. Our analyses show a sensitivity of the δT profile to the parameter associated with the surface fraction (σ_{dz}) of precipitating descents. We found that high values of σ_{dz} result in lower temperatures inside cold pools. In contrast, the variation of the other parameters

because this profile may be affected not only by the cold pool parametrization but also by its coupling

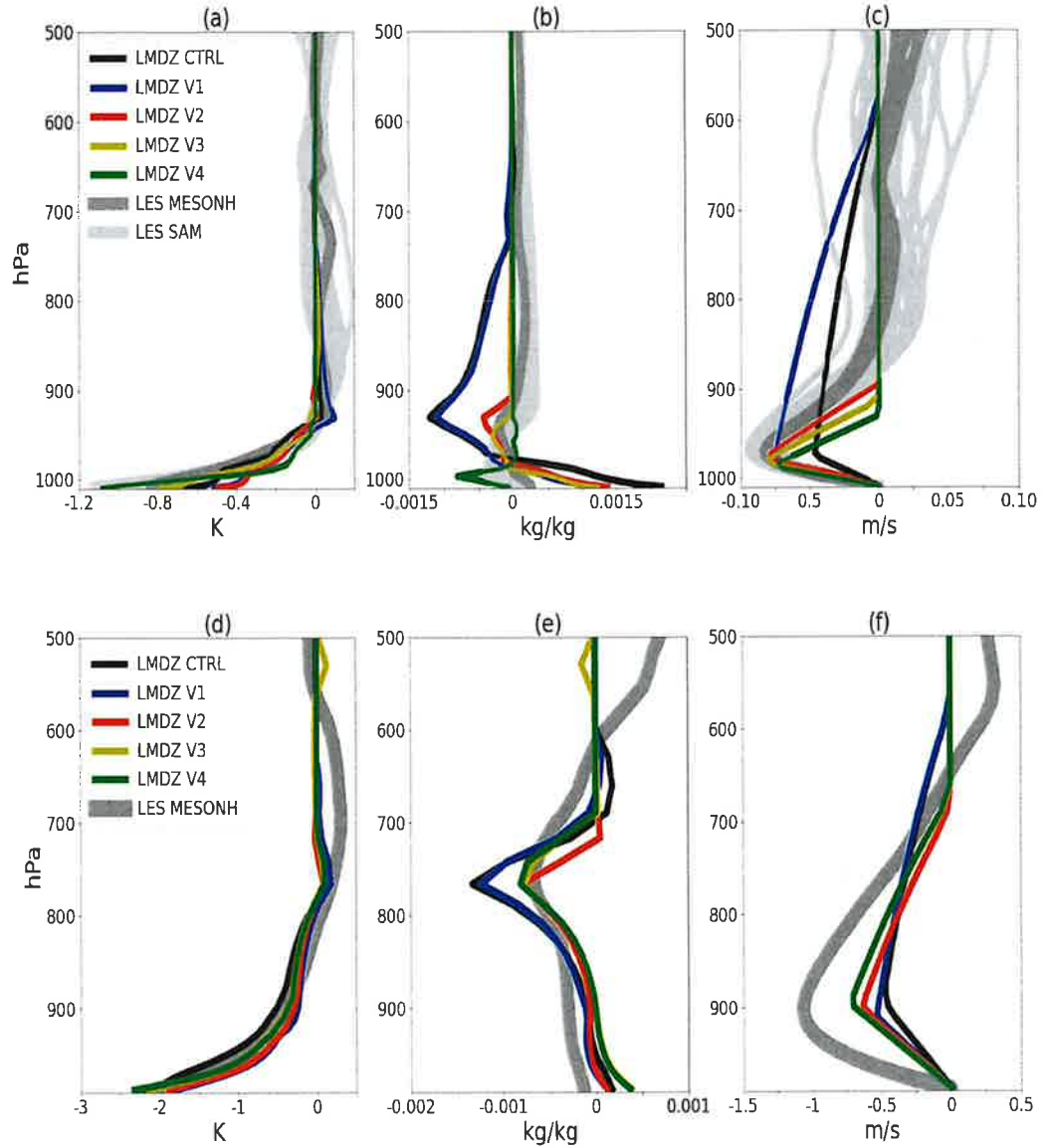


FIGURE 1.8 – Vertical profiles of δT , δq and δw calculated in the LES and simulated in the control LMDZ (~~LMDZ~~ CTRL), LMDZ with the adjustment of the coefficient k to 0.66 (~~LMDZ~~ V1), LMDZ with the drop in altitude (h_m) at which the subsidence of the air masses in cold pools is zero (~~LMDZ~~ V2), LMDZ with the adjustment of the surface fraction of the precipitating descents, σ_{dz} , to 0.02 (~~LMDZ~~ V3) and LMDZ with the activation of thermals in the entire domain (LMDZ V4) on the RCE case (a, b, c) and on the AMMA case (d, e, f).

does not affect the δT profile. Table 1.4 presents all the parameters used in tuning the δT profile. In the standard LMDZ configuration, σ_{dz} is set to 0.003. In our tuning

TABLE 1.3 – List of parameters used for tuning the δT profile

Notation	Definition
ALPBLK	efficiency on the power supplied by thermals at the convection
HTRIG	maximum height of cumulus to trigger convection
STRIG	threshold size from which a cumulus turns into a cumulonimbus
TTOPMAX	maximum temperature at the top of cumulonimbus
ELCV	maximum concentration of condensed water
SIGDZ	surface fraction covered by precipitating descents
WKPUPPER	factor connecting h_{wk} and h_m
OMPMX	
WBTOP	
WBSRF	
RQSPO	
RQSDP	
RQSTOP	
FACTAU	

tests, we assigned σ_{dz} a range of values from 0.001 to 0.08. The results show that, for the RCE case, the values of σ_{dz} providing the best fit of δT is between 0.02 and 0.05, while for the AMMA case they vary between about 0. and 0.02.

The paramètre σ_{dz} depends on the géométrie of the convective cells. Although a parameterization of σ_{dz} may be relevant, it is outside the scope of this study. Here, we take advantage of the tuning results to set an optimal value of σ_{dz} for the RCE and AMMA cases. We thus set σ_{dz} to 0.02, a value compatible with both cases.

We perform a simulation of LMDZ V3 by imposing σ_{dz} to 0.02, integrating this modification as well as the two previous ones. The analysis of the δT profile in the LMDZ V3 simulations shows a better representation of the temperature at the surface of cold pools on the RCE case (Fig. 1.8a). In the simulation of LMDZ V3, the increase of σ_{dz} leads to a more intense evaporation in the model, thus further reducing the temperatures within cold pools. The simulations of LMDZ V3 also show a slight decrease in cold pools temperatures in the AMMA case, while remaining consistent with the LES (Fig. 1.8d). The simulations of LMDZ V3 also indicate that, for the RCE and AMMA cases, increasing σ_{dz} slightly modifies the δq profiles, with a more pronounced effect at the top of cold pools, allowing to get closer to the LES at this level (1.8b and 1.8e). This highlights the role of precipitation evaporation in the variation of humidity inside cold pools.

Decision is
on more or
less tuning

1.5.4 Activation of thermals throughout the domain

The modifications made so far improve the temperature of cold pools and top humidity, but have a very limited effect on surface humidity, which remains higher in the model than in the LES for the RCE and AMMA cases. To understand this difference in surface humidity, we test enabling thermals throughout the domain, since in the standard LMDZ configuration, thermals only interact with temperature and humidity profiles outside cold pools. This choice was originally made to account for the fact that the atmosphere is more stable inside cold pools, which would inhibit convection in these regions. In the configuration, we interact thermals with the grid-averaged temperature and humidity profiles to analyze their effect on the δq profiles, starting from the V4 configuration. For the RCE case, the LMDZ V4 simulations show a clear decrease in the surface humidity of cold pools, corresponding better to the results obtained with the LES (Fig. 1.8b). This result is expected because the vertical transport by thermals systematically dries the surface (Diallo et al., 2017). We also observe, in the LMDZ V4 simulations, a modification of the δq profile at the top of cold pools for the RCE case, although it always remains comparable to the LES. On the other hand, for the AMMA case, these same simulations indicate practically no effect on the humidity of cold pools (Fig. 1.8e). This could be explained by the too short duration of the simulation on this case, which would prevent obtaining a net effect of thermals. Indeed, we tested this modification in a 3D simulation over a period of thirty days. As for the ocean, the results also show a drying of cold pools on the continent with a strong effect. These results suggest that thermals would play a key role in regulating the surface humidity of cold pools, by mixing the excess surface humidity with the dry air above. To take into account the effect of thermals in cold pools, one might wish to integrate shallow thermals, which do not generate cumulus, but simply mix the excess humid air at the surface with the dry air above.

In intermediate tests, we also studied the effect of the surface evaporation flux on the variation of the humidity at the surface of cold pools on the RCE case by activating the "splitting" in the model. Activating this mode makes it possible to differentiate the calculation of the evaporation flux between the inside and the outside of cold pools, unlike the standard configuration where this flux is treated uniformly for both regions. These tests revealed that, on the RCE case, the surface evaporation flux contributes very little to the variation of the humidity at the surface of cold pools. These tests were not carried out on the AMMA case, because the current version of LMDZ does not yet allow to calculate separately the surface evaporation flux between the inside and the outside of cold pools on the continent. But it would

be interesting to explore the impact of this evaporation flux on the variation of the humidity of cold pools in the continental case.


The simulations of LMDZ V4 also show that thermals have a fairly strong cooling effect on cold pools in the RCE case (Fig. 1.8a). This effect is not observed in the AMMA case (Fig. 1.8d). But 3D simulations also indicate a cooling of cold pools on the continent when thermals are activated in the whole domain.

TABLE 1.4 – Description of simulations performed with LMDZ in the standard configuration and with various modifications

Simulations	Protocols
LMDZ CTRL	simulation of LMDZ with the standard configuration by imposing D_{wk} to 510^{-10}
LMDZ V1	LMDZ CTRL + change of k to 0.66
LMDZ V2	LMDZ V1 + drop of h_m
LMDZ V3	LMDZ V2 + adjusting of σ_{dz} to 0.02
LMDZ V4	LMDZ V3 + activation of thermals throughout the domain

1.5.5 Effect of changes on $WAPE$, ALE_{wk} , C_* and ALP_{wk}

In this section, we compare the variables of $WAPE$, ALE_{wk} , C_* and ALP_{wk} computed in LES with those simulated by LMDZ, integrating all modifications (LMDZ V4). Although the comparisons are made directly with LMDZ V4, we will discuss in detail the impact of each modification on the results.



On the RCE case, LMDZ V4 simulates values of $WAPE$ closer to the LES than LMDZ CTRL (table 1.5). This improvement of the $WAPE$ in the model on this case is mainly linked to the better representation of the temperature inside cold pools. This also leads to a strengthening of ALE_{wk} which is closer to the LES values (table 1.5). These results indicate that the low values of $WAPE$ and ALE_{wk} simulated by LMDZ in its standard configuration on the RCE case are explained by the underestimation of the cold anomaly of cold pools on this case. On the contrary, for the AMMA case, a slight decrease in $WAPE$ is observed in the LMDZ V4 simulations, linked to the low impact of the passage from k to 0.66 on the δT profile, while remaining comparable to the LES results (table 1.5). This decrease in $WAPE$ also leads to a slight decrease in ALE_{wk} , but the values remain consistent with those of the LES (table 1.5).

Comparisons of C_* computed in LES with those simulated by LMDZ V4 show that, in the RCE case, the model reproduces spreading speed very close to those of LES

TABLE 1.5 – Comparison of the variables $WAPE$, ALE_{wk} , C_* and ALP_{wk} calculated from the samplings in the LES, with those simulated in LMDZ control (LMDZ CTRL) and with modifications (LMDZ V4)

	$WAPE$ (J/Kg)	ALE_{wk} (J/kg)	C_* (m/s)	ALP_{wk} (J/kg)
RCE				
LES SAM	7.962	10.460	2.228	0.054
LES MESONH	7.912	6.965	2.264	0.020
LMDZ CTRL	2.957	2.957	0.802	0.001
LMDZ V4	4.535	4.535	1.988	0.011
AMMA				
LES MESONH	34.250	33.480	4.939	0.982
LMDZ CTRL	30.430	30.430	2.574	0.042
LMDZ V4	21.410	21.410	4.318	0.468

(table 1.5). This improvement in the representation of C_* in the model in this case is due both to the better representation of $WAPE$ and to the adjustment of the coefficient k to 0.66. Indeed, during intermediate tests, we noticed that even with an improvement in $WAPE$, the model simulates relatively low values of C_* (1.064 ms^{-1}) compared to LES when the coefficient k is set to 0.33. In the AMMA case, the table 1.5 indicates that LMDZ V4 also simulates values of C_* quite close to those calculated in the LES. The improvement in this case is mainly attributed to the adjustment of the coefficient k to 0.66, since the model already simulated the $WAPE$ quite well in this case with the standard configuration. The results on these two cases highlight, beyond a good representation of the temperature inside cold pools, the importance of an accurate estimation of the coefficient k to better simulate the spreading speed of cold pools.

Concerning ALP_{wk} , the table 1.5 shows a clear improvement in its representation in LMDZ V4 simulations on both cases. This result is mainly attributable to the improvement of C_* .

1.6 Effect of changes on large-scale variables

Although the modifications presented above have improved the representation of cold pools in the model, it is also essential to examine their impact on large-scale variables. In this section, we analyze the effect of these adjustments on variables such as potential temperature (θ), specific humidity (qv), and cloud fraction (r_{neb}) profiles. For this, the same profiles are recalculated in the LES for the RCE and

AMMA cases and then compared with those obtained in each modified version of the LMDZ model. The profiles of θ and qv in the LES are calculated by a horizontal average of these variables over the domain, while the profile of $rneb$ is obtained by selecting the grid points where the condensed water mass exceeds 10^{-5} kg/kg.

Comparisons show that the modification of the coefficient k (LMDZ V1) has a negligible impact on the average profiles of θ , qv and $rneb$ for the RCE and AMMA cases (Fig. 1.9). In the RCE case, the decrease in h_m (LMDZ V2) slightly dries the atmosphere between 800 and 600 hPa, while the increase in σ_{dz} (LMDZ V3) induces a re-wetting, bringing the qv profile of the model closer to those of the LES in this case (Fig. 1.9b). However, the decrease in h_m has no effect on the qv profiles of the AMMA case (Fig. 1.9e) and also on the θ and $rneb$ profiles for both cases (Fig. 1.9a,c,d and f). The increase in σ_{dz} , on the other hand, cools the lower layers of the atmosphere in the RCE case due to the intensification of precipitation evaporation, which slightly moves the model away from the LES (Fig. 1.9e). In the AMMA case, the impact of this modification on the θ profile remains very limited (Fig. 1.9a), consistent with the results of section 1.5.3, where the adjustment of σ_{dz} slightly influences the temperature of cold pools for this case. In order to reduce the gap between the θ profile of the model and that of the LES in the RCE case, a tuning would be desirable. This modification of σ_{dz} also results in a slight decrease in the cloud base altitude for the RCE case (Fig. 1.9c). Figures 1.9 reveal that, for the RCE case, the activation of thermals in the entire domain (LMDZ V4) has a limited effect on the mean profiles. For the AMMA case, like the variables of cold pools model, figures 1.9 show that the activation of thermals does not affect the mean profiles.

1.7 Conclusions

In this study, we evaluated the parameterization of cold pools in the LMDZ climate model with reference to the two oceanic LES in RCE and one continental LES in the AMMA case. We evaluated both the physics embedded in the cold pools model and its internal variables, as well as those used for coupling with deep convection. For this, we first performed sampling in the LES, separating the interior and exterior of cold pools on the RCE and AMMA cases by surface temperature anomalies lower than -0.2 K and -1 K respectively, in order to calculate the targeted variables. The internal variables analyzed include the profiles of temperature (δT), humidity (δq) and vertical velocity ($\delta \omega$) differences between the inside and outside of cold pools, the collapse energy (W_{APE}), the spreading speed (C_*), as well as the Available Lifting Energy ($AL_{E_{wk}}$) and Power ($AL_{P_{wk}}$) variables related to cold pools for the

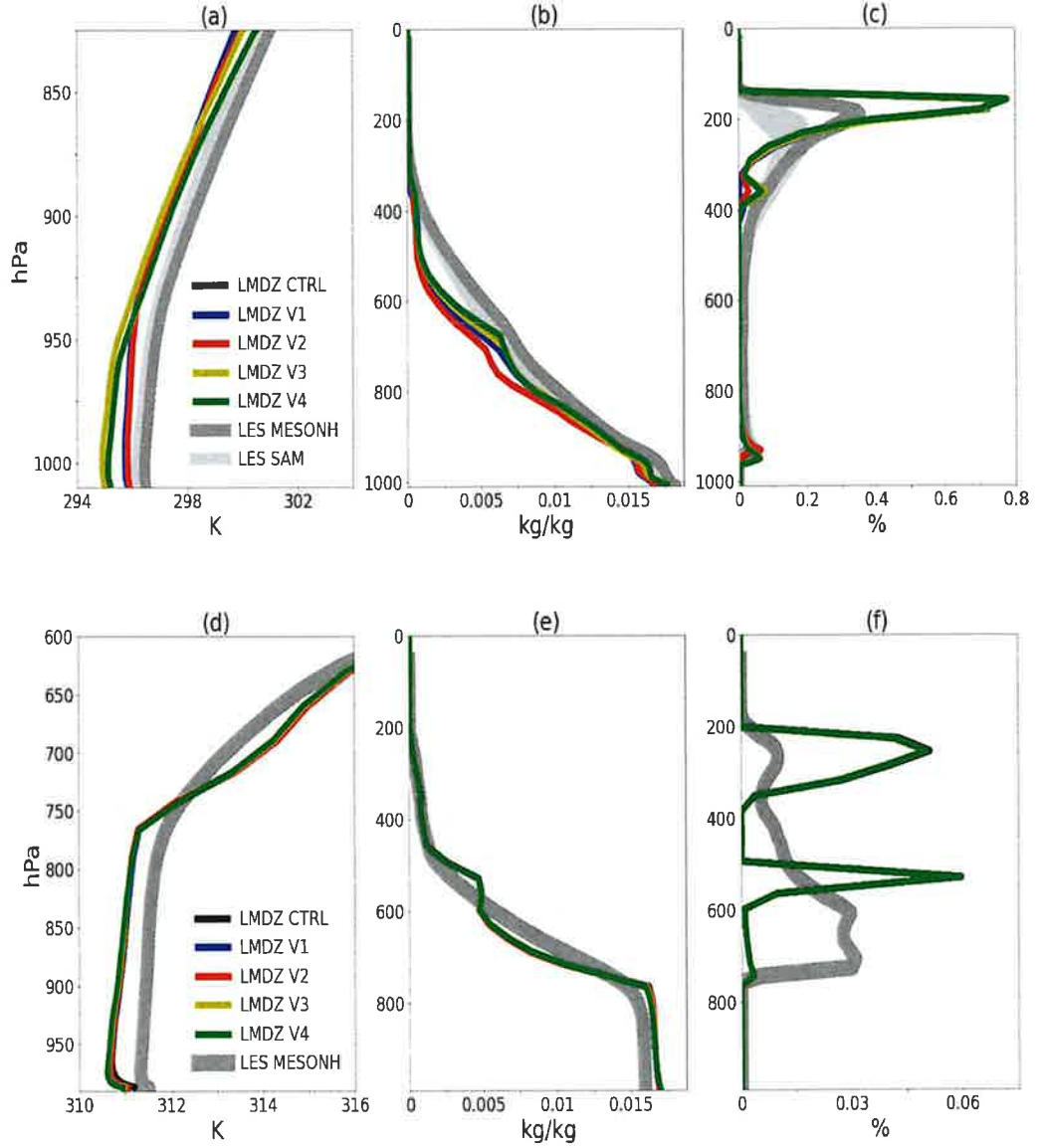


FIGURE 1.9 – Vertical profiles of potential temperature (θ), specific humidity (qv) and cloud fraction ($rneb$) calculated in the LES and simulated in control LMDZ (LMDZ CTRL), LMDZ with the adjustment of the coefficient k to 0.66 (LMDZ V1), LMDZ with the decrease in altitude (h_m) at which the subsidence of the air masses in cold pools is zero (LMDZ V2), LMDZ with the adjustment of the surface fraction of the precipitating descents, σ_{dz} , to 0.02 (LMDZ V3) and LMDZ with the activation of thermals in all the domain (LMDZ V4) on the RCE case (a, b, c) and on the AMMA case (d, e, f).

coupling with deep convection.

We first validated the physics of the cold pools model for calculations of ALE_{wk} , C_* and ALP_{wk} based on the $WAPE$. For this, these three variables were recalculated in the LES using the $WAPE$, derived from the sampled $\delta\theta_v$ profiles, according to the parameterization. The values obtained were then compared to those calculated from the divergence of wind at 10 m inside cold pools (for C_*) and the vertical velocities (w_{bgust}) at the cloud base at the gust fronts (for ALE_{wk} and ALP_{wk}), also sampled in the same LES. The results show that the ALE_{wk} calculated from the $WAPE$ is comparable to that estimated from the w_{bgust} . This result is consistent with the model hypothesis, which estimates an equality between ALE_{wk} and $WAPE$. The spreading speed (C_*), determined from the mean of divergence of wind at 10 m inside cold pools, is consistent with the estimate based on the square root of $WAPE$. The proportionality coefficient k , evaluated here at 0.66, is consistent with the work of Lafore and Moncrieff (1998), and differs from the initially assumed value of 0.33 in the model. ALP_{wk} , calculated using C_* from the $WAPE$ (with $k = 0.66$), is close to the estimate derived directly from the w_{bgust} . This result is compatible with the model hypothesis according to which ALP_{wk} translates a transformation of the horizontal power of the pockets into a vertical power, with a conversion coefficient of 25%. All of these results show the overall consistency of the model hypotheses with the three LES (RCE and AMMA) used in this study.

We then compared the variables simulated by the model to those calculated in the LES by performing a simulation with a version single-column of LMDZ for the RCE and AMMA cases, using the same initial and boundary conditions as the LES. ~~Our analyses show that the model simulates cold pools that are too dry at the top~~ compared to the LES, for ~~both the RCE and AMMA cases~~. This is due to a much higher maximum subsidence altitude (h_m) of dry air masses imposed in the initial parameterization (at 600 hPa over the ocean and the mainland) than that observed in the LES (below 800 hPa on the RCE case and below 600 hPa on the AMMA case), which increases the supply of dry air into cold pools in the model and thus reduces its humidity at the top. By lowering this altitude to a level equivalent to that observed in the LES, the representation of the humidity at the top of cold pools is significantly improved on both cases. These results highlight the significant impact of descending air masses in cold pools on the vertical humidity profile. Moreover, the ability of the model to reproduce well the humidity at the top of cold pools for both cases by changing the formulation of h_m and making it depend on the height

(h_{wk}) of the top confirms the relevance of the physical model, which postulates an impermeability of cold pools below the top and a penetration of dry air only above this level, canceling out at a certain altitude. Our results also show that, in the RCE case, the LMDZ model simulates cold pools less cold ~~er~~ compared ~~to the~~ LES. Thanks to the automatic calibration tool (HighTune), we identified this anomaly as being mainly related to the surface fraction (σ_{dz}) of the precipitating descents, set to a very low value of 0.003, which limits evaporation in the model. The tuning suggests a range of values for σ_{dz} between 0.02 and 0.05 in order to compensate for this low evaporation and to improve the representation of the temperature of cold pools in the RCE case. In this study, we adjusted σ_{dz} to 0.02 to improve δT . The tuning results, however, highlight the interest of moving towards a more physical model of this surface, which depends on the geometry of the convective cells. Our results also show that the model simulates wetter cold pools on the surface compared to LES, both in the RCE and AMMA cases, with a more marked difference in the RCE case. By making the thermals act with the average temperature and humidity profiles in the grid rather than only outside cold pools, we find that, in the RCE case, taking into account the thermals in cold pools significantly improves the representation of surface humidity. This drying effect of cold pools surface by thermals is however not observed in the AMMA case, due to the short duration of the simulation. But it is confirmed in a 3D simulation over several days that, as on the ocean, the thermals also dry the cold pools on the continent. The presence of the thermals allows the excess humidity on cold pools surface to be mixed with the dry air above, thus helping to reduce it. However, due to the stratification of cold pools, thermals present within them would be crushed at the surface and would not promote cloud formation. Our results argue for the development of a model of shallow thermals, which do not trigger cumulus, but simply ensure the mixing of excess moist air at the surface with the air above. Our results also indicate a fairly strong cooling effect of cold pools by thermals both on the ocean and on the continent. We also note that the surface evaporation flux has a very limited effect on the moisture variations at the surface of cold pools in the RCE case. We have not studied its impact in the AMMA case, because there is no method yet to calculate this flux separately on the continent. But it would be interesting to examine its influence on the moisture of the continental cold pools.

Regarding the variables WAP_E , ALE_{wk} , ALP_{wk} and C_* , our results reveal that, in the standard version of the model, WAP_E and ALE_{wk} are small in the RCE case compared to the LES, and that C_* and ALP_{wk} are underestimated for the RCE

and AMMA cases. The low values of $WAPE$ on the RCE case are explained by too high temperatures inside cold pools in the model, leading also to low ALE_{wk} . By adjusting the profile of δT with σ_{dz} to 0.02, the representation of $WAPE$ and ALE_{wk} improves significantly. The underestimation of C_* for the RCE case is related to the underestimation of the $WAPE$ and to the coefficient k set at 0.33 while on the AMMA case, it is simply due to this value of k , because the $WAPE$ is well simulated there. Adjusting k to 0.66 with a good representation of the $WAPE$ significantly improves the representation of C_* for both cases. Finally, the low values of ALP_{wk} in both cases are due to the low C_* with $k=0.33$, and the improvement of C_* allowed a better simulation of ALP_{wk} in these cases.

The impact of these modifications on large-scale variables, such as potential temperature (θ), specific humidity (qv), and cloud fraction ($rneb$), was also analyzed. For the RCE case, our results show that the decrease in h_m slightly dries the atmosphere below 800 hPa. But the increase in σ_{dz} to 0.02 favors a re-humidification of the atmosphere, allowing to get closer to the LES. However, this increase in σ_{dz} also leads to a marked cooling in the lower layers of the atmosphere, moving further away from the LES. To solve this problem, a parameter adjustment (tuning) will be considered. The other modifications have a negligible impact on the large-scale variables in the RCE case. For the AMMA case, no modification has had a major effect on these variables.

Although significant progress has been made in recent years in modeling cold pools, due to their important role in convection, challenges remain. For example, the life cycle of cold pools, including their birth, death or collisions, needs to be addressed. After highlighting the impact of thermals on humidity and temperature variations within cold pools, we encourage the development of a parameterization of thermals capable of taking into account their influence without leading to cloud formation. The issue of the propagation of cold pools from grid cell to grid cell needs to be also integrated into GCMs, as well as the wind gusts associated with their spreading.

Bibliographie